International Journal of Research in Engineering and Science (IJRES)
ISSN (Online): 2320-9364, ISSN (Print): 2320-9356
www.ijres.org Volume 10 Issue 3 ǁ 2022 ǁ PP. 72-76

Superposition Model Investigation of Mn^{2+} doped $Ni[C_4H_30_4]_2.6H_20$ Crystal

Ram Kripal, Upendra Mani Tripathi
EPR laboratory, Department of Physics, University of Allahabad, Allahabad (India)-211002

Abstract
Superposition model is employed to obtain the crystal field parameters (CFPs) of Mn^{2+} doped nickel bis (hydrogen maleate) hexahydrate, Ni $[C_4H_30_4]_2.6H_20$ (NiMH) single crystal. The zero field splitting parameters (ZFSPs) D and E are then evaluated using perturbation and microscopic spin Hamiltonian (SH) theory. The theoretical D and E show reasonable agreement with the experimental values found from electron paramagnetic resonance analysis. The results suggest that the Mn^{2+} ion enters the lattice substitutionally at Ni^{2+} site in NiMH. The method may be utilized for the modeling of other ion-host systems.
Keywords: *A. Organic compounds; A. Single Crystal; C. Crystal structure and symmetry; D. Crystal and ligand fields; D. Optical properties; E. Electron paramagnetic resonance.*
PACS No. : *76.30*

Date of Submission: 09-03-2022 Date of acceptance: 25-03-2022

I. INTRODUCTION

Superposition model (SPM) is quite useful to obtain physical and geometrical information existing in crystal field parameters of various ion-host systems [1, 2]. The positions of ligands are needed to apply this model and hence the theories of local distortion in crystals are very important. The reasonable results for $Fe^{3+}$and Mn^{2+} spin Hamiltonian parameters were found [3, 4] by using this model together with local distortion.

A number of mechanisms have been suggested for the ground state splitting of the magnetic ions introduced in crystals [5-8]. In majority of the systems, cubic field and the diagonal part of free-ion Hamiltonian are supposed to be unperturbed terms while the spin- orbit coupling, the low-symmetry field, and the off-diagonal part of free-ion Hamiltonian are taken as the perturbation terms [9].

EPR investigation of Mn^{2+} doped nickel bis (hydrogen maleate) hexahydrate, Ni $[C_4H_30_4]_2.6H_20$ (NiMH) single crystals has been reported [10]. We can consider two possibilities, substitutional and interstitial, for Mn^{2+} ion location in the NiMH crystal. It was suggested [10] that Mn^{2+} ion enters the lattice of NiMH substitutionally at Ni^{2+} site. In this study, the zero-field splitting parameters (ZFSPs) D and E are evaluated for the Mn^{2+} ion at substitutional Ni^{2+} site in NiMH; using crystal field parameters (CFPs) obtained from SPM and perturbation equations [11]. The values of D and E obtained using this model are in reasonable agreement with the experimental ones.

II. CRYSTAL STRUCTURE

The crystal structure of NiMH single crystal is isomorphous to the magnesium bis (hydrogen maleate) hexahydrate crystal. The crystals are monoclinic with space group $P2_1/c$ and Z = 2 [12]. The unit cell dimensions are a = 1.0207 nm, b = 1.1829 nm, c = 0.6745 nm and β = 104.2° [12]. Ni ion is surrounded by six water molecules and each water molecule contributes one oxygen atom to a Ni^{2+} ion forming distorted octahedron around the Ni^{2+} ion. However, due to introduction of Mn^{2+} ion in NiMH lattice, the site symmetry around Mn^{2+}ions is lowered and may be considered as approximately orthorhombic, as suggested by EPR investigation of Mn^{2+}: NiMH at room temperature [10]. The structure is shown in Fig.1.

III. THEORETICAL INVESTIGATION

The resonance magnetic fields can be obtained using the spin Hamiltonian [13, 14]

$$\mathcal{H} = g\mu_B \boldsymbol{B.S} + D\{S_z^2 - \frac{1}{3}S(S+1)\} + E(S_x^2 - S_y^2) + (\frac{a}{6})[S_x^4 + S_y^4 + S_z^4 - \frac{1}{5}S(S+1)(3S^2+3S-1)]$$

$$+ \frac{F}{180}\{35\,S_z^4 - 30\,S(S+1)S_z^2 + 25S_z^2 - 6S(S+1) + 3S^2(S+1)^2\} + \frac{K}{4}[\{7S_z^2 - S(S+1) - 5\}$$

$$(S_+^2+S_-^2)+(S_+^2+S_-^2)\{7S_z^2-S(S+1)-5\}] + \mathcal{A}S_zI_z + \mathcal{B}(S_xI_x+S_yI_y) \qquad (1)$$

where g is the isotropic spectroscopic splitting factor, μ_B is the Bohr magneton, $\boldsymbol{B}$ is the external magnetic field. D and E are the second-rank axial and rhombic ZFSPs, whereas a, F, and K are the fourth-rank cubic, axial and rhombic ones, respectively. The last two terms in Eq. (1) give the hyperfine (I = 5/2) interaction. The F and K terms are deleted as their effect is very small [13, 15, 16]. The isotropic approximation for the electronic Zeeman interaction is usually valid for $3d^5$ ions [13, 17]. The above two approximations may slightly affect the value of a [18]. The maximum overall splitting direction of EPR spectrum is taken as the z axis and that of the minimum as the x axis [19]. The laboratory axes (x, y, z) determined from EPR spectra are found to coincide with the modified crystallographic axes (CAS*), a, b, c*. The z-axis of the local site symmetry axes, i.e. the symmetry adapted axes (SAA) is along the metal oxygen bond and the other two axes (x, y) are perpendicular to the z-axis.

In NiMH, nickel ion is located within a distorted octahedron of water oxygen ions [10, 12] and the local symmetry is considered approximately orthorhombic of first kind (OR-I) [20]. In an OR-I symmetry, the ZFSPs D and E of $3d^5$ ions are found [11, 21] as:

$$D = (3\xi^2/70P^2D)(-B_{20}^2 - 21\,\xi\,B_{20} + 2B_{22}^2) + (\xi^2/63P^2G)(-5B_{40}^2 - 4B_{42}^2 + 14B_{44}^2) \qquad (2)$$

$$E = (\sqrt{6}\,\xi^2/70P^2D)(2B_{20}-21\,\xi)\,B_{22} + (\xi^2/63P^2G)(3\sqrt{10}\,B_{40} + 2\sqrt{7}\,B_{44})\,B_{42} \qquad (3)$$

where P = 7B+7C, G = 10B+5C, and D = 17B+5C; B and C are the Racah parameters. Eqs. (2) and (3) are good for weak-field cases, and are also correct for the low-symmetry components [11].

Taking the covalency effect into consideration, the B, C and ξ are given in terms of the average covalency parameter N as [22-23]

$$B = N^4B_0,\ C = N^4C_0;\ \xi_d = N^2\,\xi_d^0 \qquad (4)$$

where B_0, C_0, and ξ_d^0 are the free ion Racah and spin-orbit coupling parameters, respectively [22-23]. B_0 = 960 cm^{-1}, C_0 = 3325 cm^{-1}, ξ_d^0 = 336 cm^{-1} for free Mn^{2+} ion [13].

From optical absorption of Mn^{2+} doped crystal with water oxygen ligands [24]: B = 917cm^{-1} and C = 2254 cm^{-1}were obtained. The average value [23] of N = $\left(\sqrt{B/B_0} + \sqrt{C/C_0}\right)/2$ = 0.91 is used to find the ZFSPs D and E from Eqs. (2) and (3).

The SPM is used to compute the CFPs, B_{kq} for Mn^{2+} ion in NiMH single crystal and ZFSPs are then calculated using these CFPs.

The SPM has successfully explained the crystal-field splitting of $4f^n$ ions [25] and also of some $3d^n$ ions [26-28]. The model gives the CFPs as [11, 25]

$$B_{kq} = \sum \bar{A}_k(R_j)\,K_{kq}(\theta_j,\phi_j) \qquad (5)$$

where R_j are the distances between the Mn^{2+} ion and the ligand ion j, R_0 is the reference distance, generally taken near a value of the R_j's. θ_j give the bond angles in a chosen axis system (symmetry adapted axes system (SAAS)) [29, 30]. Summation is over all the nearest neighbour ligands. The coordination factor $K_{kq}(\theta_j$,

ϕ_j) are the explicit functions of angular position of ligand [11, 29, 31-32]. The intrinsic parameter $\overline{A_k}$ (R_j) is expressed by the power law [9, 20] as:

$$\overline{A_k}\ (R_j) = \overline{A_k}\ (R_0)\ (R_0 / R_j\ )^{t_k} \qquad (6)$$

where $\overline{A_k}$ (R_0) is intrinsic parameter for a given ion host system. The symbol t_k is power law exponent. The crystal-field parameters B_{kq} may be determined using Eq. (5) [33].

For $3d^5$ ions, $\overline{A_2}$ (R_0) / $\overline{A_4}$ (R_0) is 8 -12 [5, 27]. In this study, we have taken $\overline{A_2}$ (R_0) / $\overline{A_4}$ (R_0) = 10. For $3d^N$ ions in the 6-fold cubic coordination $\overline{A_4}$ (R_0) can be obtained from the relation: $\overline{A_4}$ (R_0) = (3/4) Dq [18]. As $\overline{A_4}$ (R_0) is independent of the coordination [34], the above relation is used to find $\overline{A_4}$ (R_0) with Dq = 756 cm^{-1} [24].

IV. RESULT AND DISCUSSION

Firstly to check the substitution at Ni^{2+} site, the origin of Mn^{2+} was shifted at the Ni^{2+} ion. As the ionic radius of the impurity Mn^{2+} ion (0.080 nm) is slightly larger than that of the host Ni^{2+} (0.069 nm), a distortion is expected [35]. From the coordinates x, y, z; the bond distances of different ligands, R_j together with the angles θ_j and ϕ_j are calculated and are given in Table 1. In adjusting the Mn-O distances to match the experimental values, the site symmetry is preserved as well as the energy is minimized and so the structural stability is taken into account. Taking R_0 as slightly smaller than the minimum of R_j [36], i.e. R_0 = 0.155 nm, $\overline{A_2}$ (R_0) / $\overline{A_4}$ (R_0) = 10, t_2= 3, t_4= 5 [5]; taking no distortion, we obtain B_{kq} and then |D| and |E| which are inconsistent with the experimental values as shown in Table 2. Therefore, we have considered the distortion. The bond distances of different ligands R_j and the angles θ_j and ϕ_j calculated for this case are also given in Table 1. The calculated B_{kq} from Eq. (5) and transformation S2 for standardization [19] as well as ZFSPs |D| and |E| taking other parameters as above are presented in Table 2. From Table 2, |D| and |E| are in reasonable agreement with the experimental values when distortion is taken into consideration. Such type of model calculations have been done earlier in case of Mn^{2+} and Fe^{3+} doped anatase TiO_2 crystal [37]. We have also studied the interstitial sites for Mn^{2+} ions. The obtained ZFSPs come out to be inconsistent with the experimental values and so are not given here.

Using CFA program and calculated CFPs [38] with OR-I symmetry of the crystal field the optical absorption spectra of Mn^{2+} doped NiMH crystals are computed. The energy levels of the Mn^{2+} ion are found by diagonalizing the complete Hamiltonian within the $3d^N$ basis of states in the intermediate crystal field coupling scheme. The calculated energy values are given in Table 3 along with the experimental values for comparison. From Table 3 a reasonable agreement between the two is obtained. Thus, the result found using SPM with distortion support the experimental observation that Mn^{2+} ions substitute at Ni^{2+} site in the NiMH crystal [10].

V. CONCLUSIONS

The zero field splitting parameters (ZFSPs) have been evaluated using the superposition model and perturbation formulae. The calculated ZFSPs for Mn^{2+} ion in NiMH single crystal at the substitutional Ni^{2+} site are in reasonable agreement with the experimental ones. We conclude that the Mn^{2+} ion occupies substitutional Ni^{2+} site in NiMH crystal .The theoretical results support the reported experimental observation.

ACKNOWLEDGEMENT

The authors are thankful to the Head, Department of Physics, University of Allahabad for providing the facilities of the department and to Prof. C. Rudowicz, Faculty of Chemistry, Adam Mikowicz. University, Poznan, Poland for providing CFA computer program.

REFERENCES:

[1]. M. I. Bradbury, D. J. Newman, Chem. Phys. Lett. **1** (1967) 44-45.
[2]. D. J. Newman, J. Phys. C: Solid State Phys. **10** (1977) L315-L318.
[3]. E. Siegel and K. A. M $\ddot{u}$ ller, Phys. Rev. B **20** (1979)3587-95.
[4]. Y. Y. Yeung, J. Phys. C: Solid State Phys. **21**(1988)2453-61.
[5]. T. H. Yeom, S. H. Choh, M. L. Du, J. Phys.: Condens. Matter **5** (1993) 2017-2024.

[6]. M. L Du, M. G. Zhao, J. Phys. C: Solid State Phys. **18** (1985) 3241-3248.
[7]. W. L. Yu, Phys. Rev. **B 39** (1989) 622-632.
[8]. M. G. Brik, C. N. Avram, N. M Avram, Physica **B 384** (2006) 78-81.
[9]. Z. Y. Yang, J. Phys.: Condens. Matter **12** (2000) 4091-4096.
[10]. R. M. Krishna, V. P. Seth, R. S. Bansal, I. Chand, S. K. Gupta, J. J. Andre, Spctrochim. Acta A54 (1998) 517-521.
[11]. W. L. Yu, M.G. Zhao, Phys. Rev. B **37** (1988) 9254-9267.
[12]. F. Vanhoutenghem, A.T. H. Lenstra and P. Schweiss, Acta Cryst. B 43 (1987) 523-528.
[13]. A. Abragam, B. Bleaney, EPR of Transition Ions, Clarendon Press, Oxford (1970), 1970.
[14]. C. Rudowicz, Magn. Reson. Rev. **13** (1987) 1-89.
[15]. C. Rudowicz, H. W. F. Sung, Physica B, **300** (2001) 1-26.
[16]. C. J. Radnell, J. R. Pilbrow, S. Subramanian, M. T. Rogers, J. Chem. Phys. **62** (1975) 4948-4952.
[17]. J. A. Weil, J. R. Bolton, Electron Paramagnetic Resonance: Elementary Theory and Practical Applications, 2nd Edition, Wiley, New York, 2007.
[18]. C. Rudowicz, S. B. Madhu, J. Phys.: Condens. Matter **11** (1999) 273-288.
[19]. C. Rudowicz and R. Bramley, J. Chem. Phys. **83**(1985) 5192-5197; R. Kripal, D. Yadav, C. Rudowicz and P. Gnutek, J. Phys. Chem. Solids, **70**(2009) 827-833.
[20]. C. Rudowicz, Y. Y. Zhao, W. L. Yu, J. Phys. Chem. Solids **53**(1992)1227-1236.
[21]. W. L. Yu, M. G. Zhao, Phys. Stat. Sol. (b) **140** (1987) 203-212.
[22]. C. K. Jorgensen, Modern Aspects of Ligand Field Theory, North- Holland, Amsterdam, 1971, p 305.
[23]. M. G. Zhao, M. L. Du, G. Y. Sen, J. Phys. C: Solid State Phys. **20** (1987) 5557-5572; Q. Wei, Acta Phys. Polon. A**118** (2010)670-672.
[24]. R. Kripal, H. Govind, S. K. Gupta, M. Arora, Physica B, 392 (2007) 92-98.
[25]. D. J. Newman, Adv. Phys. **20** (1970) 197-256.
[26]. Y. Y. Yeung, D. J. Newman, Phys. Rev. **B 34** (1986) 2258-2265.
[27]. D. J. Newman, D. C. Pryce, and W. A. Runciman, Am. Miner. **63** (1978) 1278-1281.
[28]. G. Y. Shen, M. G. Zhao, Phys. Rev. **B 30** (1984) 3691-3703.
[29]. D. J. Newman and B. Ng, Rep. Prog. Phys. **52** (1989) 699-763.
[30]. M. Andrut, M. Wildner, C. Rudowicz, Optical Absorption Spectroscopy in Geosciences, Part II: Quantitative Aspects of Crystal Fields, Spectroscopic Methods in Mineralogy (EMU Notes in Mineralogy, Vol. **6**, Ed. A. Beran and E. Libowitzky, Eötvös University Press, Budapest, Chapter 4, p.145-188, 2004.
[31]. C. Rudowicz, J. Phys. C: Solid State Phys. **18**(1985)1415-1430; **20**(1987) 6033-6037.
[32]. M. Karbowiak, C. Rudowicz, P. Gnutek, Opt. Mater. (2011) doi: 10.1016/j.optmat.2011.01.027.
[33]. K. T. Han, J. Kim, J. Phys.: Condens. Matter **8** (1996) 6759-6767.
[34]. P. Gnutek, Z. Y. Yang, C. Rudowicz, J. Phys.: Condens. Matter **21** (2009) 455402-455412.
[35]. V. V. Laguta, M. D. Glinchuk, I. P. Bykov, J. Rosa, L. Jastrabik, M. Savinov, Z. Trybula, Phys. Rev. **B61** (2000)3897-3904.
[36]. C. Rudowicz, Y. Y. Zhou, J. Magn. Magn. Mater. **111**(1992) 153-163.
[37]. M. Acikgöz, P. Gnutek, C. Rudowicz, Chem. Phys. Letts. **524** (2012)49-55.
[38]. Y. Y. Yeung, C.Rudowicz, J. Comput. Phys. 109 (1993) 150-152.

TABLE AND FIGURE CAPTIONS:

Table 1. Coordinates of oxygen ligands, Mn-oxygen bond distances R_j and coordination angles θ_j and ϕ_j for Mn^{2+} ion doped NiMH single crystals.
Table 2. CFPs and ZFSPs calculated by the superposition model for Mn^{2+} ion doped NiMH single crystal with experimental values.
Table 3. Experimental and calculated (CFA package) energy band positions of Mn^{2+} doped NiMH single crystal.
Fig. 1: Coordination around Mn^{2+} in NiMH single crystal.

Table 1

Position of Mn^{2+}	Ligands	Spherical co-ordinates of ligands								
		x	y	z	R(nm)		θ^0		φ^o	
		(Å)								
	Without distortion									
Site I: Substitutional Mg (0, 0, 0)	O(W1)	-0 .1391	0.0065	0.1775	0.2071	R_1	85.08	θ_1	93.86	φ_1
	O(W2)	-0.0077	0.173	-0.0231	0.2058	R_2	90.64	θ_2	90.21	φ_2
	O(W3)	0.1602	0.0102	0.2556	0.2067	R_3	82.89	θ_3	85.52	φ_3
	O(W1')	0.1391	-0.0065	-0.1775	0.2071	R_4	94.91	θ_4	86.13	φ_4
	O(W2')	0.0077	-0.1735	0.0231	0.2058	R_5	89.35	θ_5	89.78	φ_5
	O(W3')	-0.1602	-0.0102	-0.2556	0.2067	R_6	97.10	θ_6	94.47	φ_6
	With distortion									
	O(W1)				0.2871 $R_1+\Delta R_1$					
	O(W2)				0.2864 $R_2+\Delta R_2$					
	O(W3)				0.2967 $R_3+\Delta R_3$					
	O(W1')				0.2971 $R_4+\Delta R_4$					
	O(W2')				0.2958 $R_5+\Delta R_5$					

OW3')		$0.2967\ R_6+\Delta R_6$

Table 2

Site	R_0(nm)	Crystal- field parameters (cm^{-1}) B_{20}	B_{22}	B_{40}	B_{42}	B_{44}	Zero-field splitting parameters ($\times10^{-4}cm^{-1}$) |D|	|E|	|E|/|D|
			Without distortion						
Site I									
$\frac{A_2}{A_4}$ =10	0.155	-14045.6	-17345.2	2247.323	2389.951	4958.178	2589	1291	0.498
			With distortion						
Site I									
$\frac{A_2}{A_4}$ =10	0.155	5491.05	4337.64	391.509	416.2247	2728.733	216.2	53.1	0.245
							Exp. 216	96.3	0.445

Table 3

Transition from $^6A_{1g}(S)$	Observed wave number (cm^{-1})	Calculated wave number (cm^{-1})
$^4T_{1g}(G)$	16044	
$^4T_{2g}(G)$	20433	19626, 19653, 20195, 20221, 20979, 20987
$^4E_g(G)$	24108	22551, 23482
$^4A_{1g}(G)$	24242	23504
$^4T_{2g}(D)$	26724	26550, 26567, 26617, 26634, 27000, 27286
$^4E_g(D)$	30451	30439, 30549
$^4T_{1g}(P)$	33956	32208, 32502, 32792, 32963, 33925, 34392
$^4A_{2g}(F)$	36846	36964
$^4T_{1g}(F)$	38521	38122, 38218, 38230, 38323, 38356, 38557

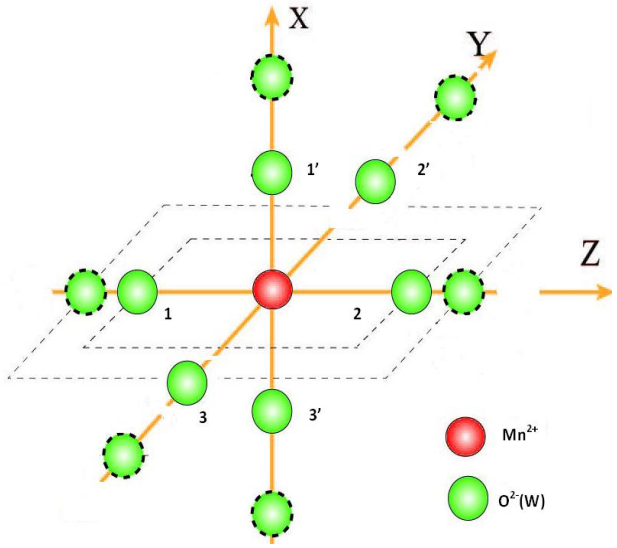

Fig.1